Search for the pseudoscalar Higgs boson A_0 of the bestest little Higgs model at the LHC and FCC-hh

Y. Cervantes-Baltazar,[1,*] E. Cruz-Albaro,[1,†] A. Gutiérrez-Rodríguez,[1,‡] M. A. Hernández-Ruíz,[2,§] and D. Espinosa-Gómez[3,‖]

[1]*Facultad de Física, Universidad Autónoma de Zacatecas, Apartado Postal C-580, 98060 Zacatecas, México*

[2]*Unidad Académica de Ciencias Químicas, Universidad Autónoma de Zacatecas, Apartado Postal C-585, 98060 Zacatecas, México*

[3]*Facultad de Ciencias Físico Matemáticas, Universidad Michoacana de San Nicolás de Hidalgo Avenida Francisco J. Mújica S/N, 58060, Morelia, Michoacán, México*

(Received 1 July 2025; accepted 2 January 2026; published 21 January 2026)

We analyze the sensitivity of the Large Hadron Collider (LHC) and the Future Circular Collider-hadron-hadron (FCC-hh) to the existence of pseudoscalar Higgs boson A_0 predicted by the bestest little Higgs model. We study the tree-level (two and three body) and one-loop decays of the pseudoscalar, $A_0 \to b\bar{b}, t\bar{t}, \gamma t\bar{t}, \gamma b\bar{b}, Zt\bar{t}, Zb\bar{b}, Wt\bar{b}, h_0 t\bar{t}, h_0 b\bar{b}$, and $A_0 \to \gamma\gamma, \gamma Z, ZZ, gg, WW$, respectively. In addition, we perform a phenomenological study of the production of the pseudoscalar A_0 via gluon-fusion $gg \to A_0 \to Y$ processes, where $Y \equiv b\bar{b}, t\bar{t}, \gamma\gamma, \gamma Z, ZZ, gg, WW$. From the cross section of the processes of interest and the expected integrated luminosity of the LHC and FCC-hh, we determined the number of events that could be produced in both colliders.

DOI: 10.1103/85b6-2w1t

I. INTRODUCTION

The discovery of a Higgs boson with a mass of 125 GeV by the ATLAS [1] and CMS [2] Collaborations at the CERN LHC has motivated the search for new exotic states at current and future colliders. Another significant fact is the recent observation of the production of four top quarks in proton-proton collisions at a center-of-mass energy of 13 TeV [3,4]. This is one of the rarest processes in the Standard Model (SM) that is currently accessible at hadron colliders. The top quark, the heaviest elementary particle in the SM, has strong connections to the SM Higgs boson and new particles predicted in theories beyond the SM (BSM). Many of these new heavy particles can decay into top quarks, resulting in the production of four top quarks via intermediate exotic particles. Such a signature could indicate the existence of new BSM particles.

The unsolved puzzles of the SM (such as dark energy, dark matter, neutrino masses, and the matter-antimatter asymmetry, among others) require new BSM physics. Many of these theories necessitate a richer Higgs sector. This extended sector is a common feature of several extended models. The Higgs sector itself has become a fundamental tool in the search for new physics, which could manifest in various ways. For example, the discovery of additional Higgs bosons or the measurement of new sources of CP violation in the scalar sector would provide direct evidence of BSM physics [5]. So far, both direct and indirect searches for new physics have produced unsuccessful results. However, it is expected that the scope of these searches will expand considerably in the future, as colliders will operate at such high energy scales that new signal channels will open up which would be suppressed at lower energies. The discovery of new non-SM Higgs bosons would be a clear sign of BSM physics with extended sectors.

Several extended models have been proposed to address open issues in the SM scenario, such as the hierarchy problem [6]. This problem is also known as the fine-tuning problem. Among the BSM models, there are little Higgs-type models [7–11] that introduce enough new physics to generate cancellations and preserve a light Higgs boson.

*Contact author: yahiralejandro.708805@fisica.uaz.edu.mx
†Contact author: elicruzalbaro88@gmail.com
‡Contact author: alexgu@fisica.uaz.edu.mx
§Contact author: mahernan@uaz.edu.mx
‖Contact author: david.espinosa@umich.mx

Published by the American Physical Society under the terms of the Creative Commons Attribution 4.0 International license. Further distribution of this work must maintain attribution to the author(s) and the published article's title, journal citation, and DOI. Funded by SCOAP³.

These models implement the idea that the Higgs boson is a pseudo-Goldstone boson. Little Higgs theories are constructed by embedding the SM within a larger group with an extended symmetry. From a phenomenological point of view, this symmetry requires the existence of new particles whose couplings ensure that large contributions to the Higgs mass cancel out. Thus, the Higgs boson mass is protected from radiative corrections. Although little Higgs models offer an attractive solution to the hierarchy problem, many of them exhibit certain theoretical inconsistencies [12]. For example, the mechanism used to generate a Higgs quartic coupling leads to violations of custodial symmetry. They are also strongly constrained by electroweak precision data in the gauge sector.

The bestest little Higgs model (BLHM) [13–15] was formulated to resolve the theoretical inconsistencies found in most little Higgs theories. This model introduces separate symmetry-breaking scales, f and F, where $F > f$. In this way, the new heavy quarks ($B, T, T_5, T_6, T^{2/3}, T^{5/3}$) acquire masses proportional to the f scale, while the new gauge bosons (Z', $W'^{\pm}$) acquire masses proportional to a combination of the f and F scales. These gauge boson partners allow the model to evade the constraints imposed by electroweak precision measurements. A successful quartic Higgs coupling is also generated without introducing any dangerous singlet in the scalar sector [12], in contrast to other little Higgs models. Instead, an additional singlet (satisfying certain additional symmetries) and a custodial $SU(2)$ symmetry [13]. The scalar sector of the BLHM has a rich phenomenology that generates neutral and charged scalar fields: $h_0, H_0, A_0, \phi^0, \eta^0, H^{\pm}, \phi^{\pm}$, and $\eta^{\pm}$. We recommend that interested readers refer to Refs. [16–18] for more information on the BLHM.

In the framework of the BLHM, the pseudoscalar Higgs boson A_0 arises as a pseudo–Nambu-Goldstone boson (pNGB) and is a CP-odd scalar whose mass is a free parameter of the scalar potential. Since the BLHM is structurally equivalent to a type-I two-Higgs doublet model (2HDM), five physical Higgs bosons are predicted: three neutral Higgs bosons ($h_0; H_0; A_0$) and two charged Higgs bosons ($H^{\pm}$). These Higgs states exhibit features similar to those of the 2HDM, but with couplings modified by the presence of new heavy quarks and gauge bosons characteristic of the BLHM; in other words, their properties are determined by the underlying symmetry structure of the model. Should any of these new particles be discovered, the next step would be to measure their properties, such as their mass, decay modes, and interaction strengths. If experimental measurements are consistent with the theoretical predictions of the BLHM or of another pNGB model, one could confirm or exclude their association with that framework. Otherwise, any deviation would point toward the existence of new physics and the need to explore alternative theoretical models capable of explaining the observed properties.

At present, experimental searches for the Higgs bosons A_0 and H_0 are conducted by the ATLAS and CMS Collaborations at the LHC. These include, for example, the $A_0/H_0 \to t\bar{t}$ channel in single-lepton and dilepton final states [19,20], the associated production with top quarks ($pp \to A_0/H_0 t\bar{t}$) [21–23], as well as the $A_0/H_0 \to b\bar{b}$ and $A_0/H_0 \to \tau^+\tau^-$ channels [20,24], among others [25,26]. Other particles predicted by the BLHM are also being searched for in the experiments, such as the heavy quark with electric charge 5/3 ($T^{5/3}$) [27–29], as well as the top and bottom partners [29,30], T and B, respectively. Regarding the latter, a search is presented for pair production of heavy T and B quarks in proton-proton collisions at $\sqrt{s} = 13$ TeV [30]. The data sample corresponds to an integrated luminosity of 35.9 fb^{-1}, collected with the CMS detector at the CERN LHC. Pair production of T quarks would result in a wide range of final states, since T quarks of charge $2e/3$ are predicted to decay to bW, tZ, and th. Likewise, B quarks are predicted to decay to tW, bZ, and bh. In another paper [31], the authors present a search for the single production of heavy quark T with subsequent decays into $T \to ht$ with $h \to b\bar{b}$ or $T \to Zt$ with $Z \to q\bar{q}$. The search utilizes a dataset of pp collisions at $\sqrt{s} =$ 13 TeV collected with the ATLAS detector, corresponding to an integrated luminosity of $\mathcal{L} = 139$ fb^{-1}. In Ref. [32], a search for pair-produced heavy T and B quarks, with electric charge $+2/3$ and $-1/3$, respectively, is performed in events with exactly one isolated lepton, at least four jets including one that is b-tagged, and high missing transverse momentum. The analysis is based on data collected by the ATLAS experiment in $\sqrt{s} = 13$ TeV proton–proton collisions at the LHC, corresponding to an integrated luminosity of 139 fb^{-1}. Several neural networks are trained for various branching ratios of the T and B quarks, assuming decays into a W, Z, or Higgs boson and a third-generation quark. The analysis considers all possible decays of the heavy quarks, but it is most sensitive to the $T \to Zt$ and $B \to Wt$ decay modes. Since the analysis does not distinguish between particles and antiparticles, the limits for $B \to Wt$ also apply to a heavy quark X with electric charge $+5/3$. On the other hand, in the category of gauge bosons, the Z' boson is not only predicted within the framework of the BLHM but also arises in several other beyond the SM scenarios. It is essential to highlight that the LHC, through the ATLAS and CMS experimental collaborations, has reported exclusion limits for the mass of Z' gauge bosons, which in some cases exceed approximately 3.9 TeV [33,34]. However, models with weaker gauge couplings yield lower mass exclusion limits [33,35]. Regarding the Z' gauge boson predicted by the BLHM, its mass is proportional to $\sqrt{f^2 + F^2}$, which is consistent with the current experimental bounds reported by ATLAS and CMS.

In this work, we investigate the production of the pseudoscalar Higgs boson A_0 via gluon fusion at current

and future colliders, such as the LHC [36–39] and the FCC-hh [40–43]. Specifically, we discuss searching for pseudoscalar A_0 decays into fermions and gauge bosons (VV, where $V = \gamma$, Z, W, g) within the context of the BLHM. Although $A_0 \to VV$ decay is an induced process at one-loop level, we believe the pseudoscalar could also be detected in a two-photon final state, similar to the discovery of the SM Higgs boson [2,44,45]. Searches in the diphoton channel are especially useful as it offers the best mass resolution and an exceptionally clean signal because the CMS and ATLAS detectors reconstruct photons with high precision. However, even if the pseudoscalar Higgs A_0 is discovered in other final states, the other possible decays must be confirmed or excluded. Thus, this study will provide information about the BLHM and the potential detection of the pseudoscalar A_0 at the LHC and the future 100 TeV collider. Our analysis does not necessarily identify A_0 as the first discovery signal, but it does provide a valuable framework for determining whether an observed new scalar belongs to a pNGB model, such as the BLHM or to another BSM scenario. The search for A_0 offers a realistic pathway toward its potential discovery, as extensive searches for this particle are currently underway at existing colliders. Moreover, the study of the pseudoscalar within the BLHM yields complementary results to the search for additional Higgs bosons in the 2HDM.

The present paper provides a rigorous investigation of the total production and the potential discovery of the pseudoscalar particle A_0, through the signal processes $gg \to A_0 \to t\bar{t} \to WbW\bar{b} \to X_W b\bar{b}$ (X_W denotes the leptonic ($l^+\nu_l l^-\bar{\nu}_l$), semileptonic ($l^+\nu_l qq'$), and hadronic ($qq'qq'$) decay channels) and $gg \to A_0 \to WW \to X_W$. While much more phenomenological study of the proposed processes is needed, we provide the necessary theoretical and phenomenological foundations for a more comprehensive and in-depth investigation. Additionally, a significant collider phenomenology study, undoubtedly, would be beneficial critical to include an analysis of the final signal and SM background, much more comprehensive than the one presented in our article.

The physics programs of current and future hadron, lepton, and hybrid colliders include, among their research objectives, the theoretical, phenomenological, and experimental study of exotic particles, such as the pseudoscalar A_0 predicted by several extensions of the SM. One of these extensions is the BLHM. For further information on studies of the pseudoscalar within other BSM frameworks, we recommend that interested readers consult Refs. [46–49]. Experimental searches for pseudoscalar Higgs bosons are essential, as they provide complementary information to theoretical predictions and help constrain the parameter space of BSM models [50,51].

The article is organized as follows. In Sec. II, we present the analytical calculations of the tree-level and one-loop decays of the pseudoscalar Higgs boson A_0. In Sec. III, the numerical results are discussed. Finally, conclusions are presented in Sec. IV. The effective couplings involved in our calculations are provided in the Appendix.

II. PSEUDOSCALAR A_0 DECAYS IN THE BLHM

In this section, we determine the partial decay widths of the pseudoscalar A_0, or otherwise provide the corresponding transition amplitudes. In this regard, we will consider direct search channels with final states of the SM. In the following, we describe the different decay modes of the Higgs boson pseudoscalar A_0.

A. Two-body decays at tree level

The Feynman diagrams corresponding to the tree-level two-body decays of the pseudoscalar A_0 are shown in Fig. 1. To obtain the analytical expressions for the decay widths, we use the Feynman rules for the interaction vertices as given in Refs. [18,52–54], with the corresponding effective couplings detailed in the Appendix. Next, in Eqs. (1) and (2) we provide the resulting expressions for the partial decay widths

$$\Gamma(A_0 \to t\bar{t}) = \frac{N_C g^2_{A_0 tt} m_{A_0}}{8\pi}\left(1 - \frac{4m_t^2}{m_{A_0}^2}\right)^{1/2}, \tag{1}$$

$$\Gamma(A_0 \to b\bar{b}) = \frac{N_C g^2_{A_0 bb} m_{A_0}}{8\pi}\left(1 - \frac{4m_b^2}{m_{A_0}^2}\right)^{1/2}. \tag{2}$$

The color factor of the quarks is represented by N_C in these expressions, while the effective couplings are denoted by $g_{A_0 tt}$ and $g_{A_0 bb}$ (see the Appendix).

B. Three-body decays at tree level

Tree-level three-body decays are fundamental processes in particle physics, as they correspond to the leading-order contributions in the perturbative expansion and can yield significant effects in various scenarios. In the context of the BLHM, the Feynman diagrams corresponding to the three-body decays of the pseudoscalar A_0 are shown in Fig. 2. For these processes, we provide only the decay amplitudes, since the analytical expressions for the decay widths are typically very lengthy. Moreover, the associated phase space is more complex, involving nontrivial multidimensional integrations. The analytical expressions for the decay

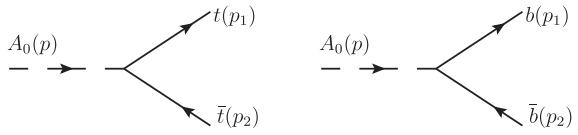


FIG. 1. Feynman diagrams corresponding to the tree-level two-body decays of the pseudoscalar A_0.

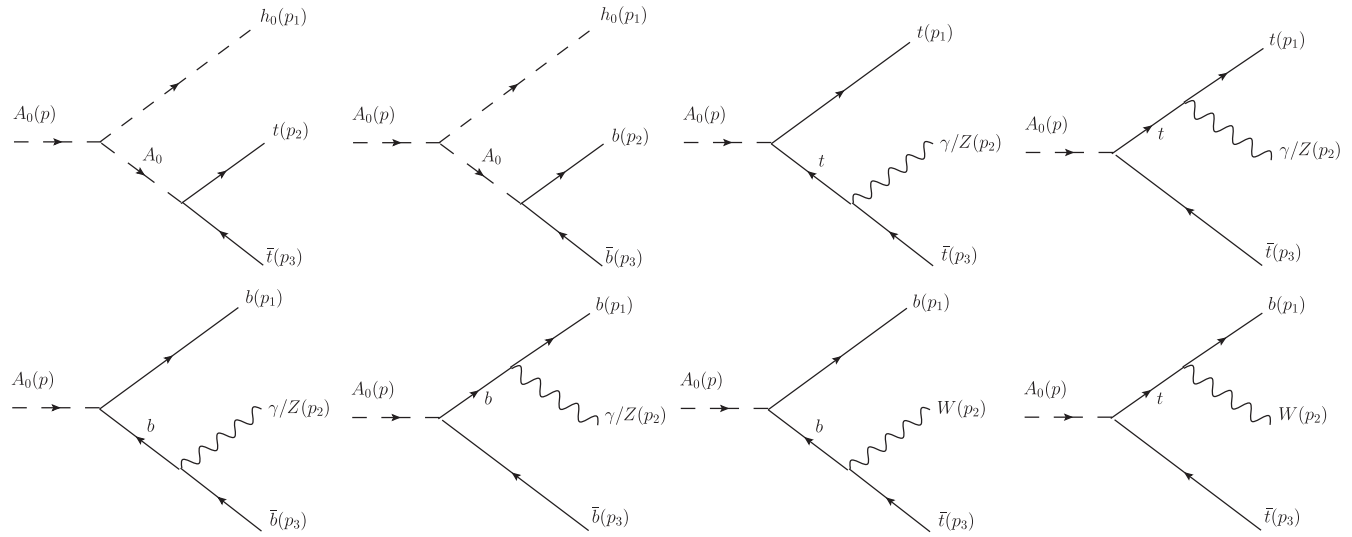


FIG. 2. Feynman diagrams corresponding to the tree-level three-body decays of the pseudoscalar A_0.

amplitudes are calculated using the generic formula described in Eq. (3) [55–57]

$$\frac{d\Gamma(A_0 \to ABC)}{dx_a dx_b} = \frac{m_{A_0}}{256\pi^3}|\mathcal{M}(A_0 \to ABC)|^2. \tag{3}$$

From the Feynman diagrams (see Fig. 2), we derive the following generic amplitudes:

$$\mathcal{M}(A_0 \to h_0 q_i \bar{q}_i) = g_{A_0 A_0 h_0} g_{A_0 q_i q_i} \left(\frac{i}{k^2 - m_{A_0}^2}\right) \bar{u}(p_2)\gamma^5 v(p_3), \tag{4}$$

$$\mathcal{M}(A_0 \to \gamma q_i \bar{q}_i) = g_{A_0 q_i q_i} g_{\gamma q_i q_i} \left[\bar{u}(p_1)\gamma^5 \left(\frac{i(-\not{k} + m_{q_i})}{k^2 - m_{q_i}^2}\right)\gamma^\mu v(p_3) + \bar{u}(p_1)\gamma^\mu \left(\frac{i(\not{k} + m_{q_i})}{k^2 - m_{q_i}^2}\right)\gamma^5 v(p_3)\right]\epsilon_\mu^*(p_2), \tag{5}$$

$$\begin{aligned}\mathcal{M}(A_0 \to Z q_i \bar{q}_i) = g_{A_0 q_i q_i} g_{Z q_i q_i} \Bigg[&\bar{u}(p_1)\gamma^5 \left(\frac{i(-\not{k} + m_{q_i})}{k^2 - m_{q_i}^2}\right)\gamma^\mu (g_V^{Z q_i q_i} + g_A^{Z q_i q_i}\gamma^5) v(p_3) \\ &+ \bar{u}(p_1)\gamma^\mu (g_V^{Z q_i q_i} + g_A^{Z q_i q_i}\gamma^5) \left(\frac{i(\not{k} + m_{q_i})}{k^2 - m_{q_i}^2}\right)\gamma^5 v(p_3)\Bigg]\epsilon_\mu^*(p_2),\end{aligned} \tag{6}$$

$$\begin{aligned}\mathcal{M}(A_0 \to W b \bar{t}) = g_{A_0 b b} g_{W b t} \Bigg[&\bar{u}(p_1)\gamma^5 \left(\frac{i(-\not{k} + m_b)}{k^2 - m_b^2}\right)\gamma^\mu P_L v(p_3) \\ &+ \bar{u}(p_1)\gamma^\mu P_L \left(\frac{i(\not{k} + m_t)}{k^2 - m_t^2}\right)\gamma^5 v(p_3)\Bigg]\epsilon_\mu^*(p_2).\end{aligned} \tag{7}$$

In these equations, q_i denotes the top and bottom quarks, while $g_V^{Z q_i q_i}$ and $g_A^{Z q_i q_i}$ represent the vector and axial-vector coupling constants of the Z boson with the q_i quarks, respectively. The effective couplings involved in Eqs. (4)–(7) together with the vector and axial-vector couplings, are provided explicitly in the Appendix.

C. Two-body decays at one-loop level

Radiative corrections at one-loop level are important processes in particle physics. They allow us to study quantum effects not observed at tree level and make more accurate predictions. Thus, for the pseudoscalar of interest, we determine the contributions of the partial decay widths of the $A_0 \to \gamma\gamma, \gamma Z, ZZ, gg, WW$ processes that arise at one-loop level [see

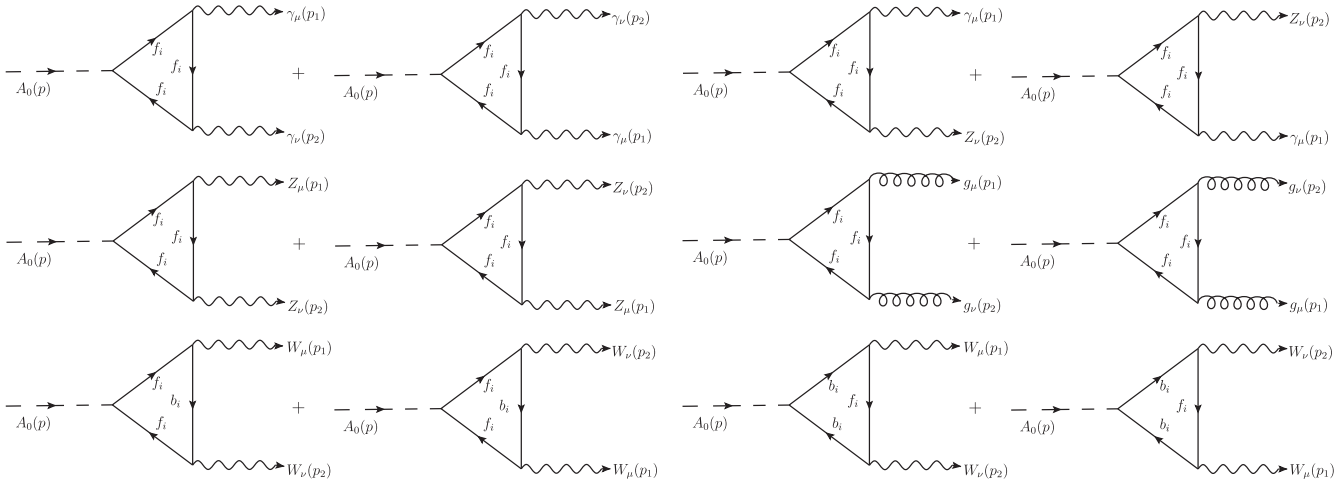


FIG. 3. Feynman diagrams corresponding to the two-body decays of the pseudoscalar A_0 at one-loop level where $f_i \equiv b, t, T, T_5, T_6, T^{2/3}$, and $b_i \equiv b, B$.

Eqs. (8)–(12)]. Figure 3 shows the Feynman diagrams associated with the $A_0 \to \gamma\gamma, \gamma Z, ZZ, gg, WW$ decays that are mediated by SM and BLHM fermions: $f_i \equiv b, t, T, T_5, T_6, T^{2/3}$, and $b_i \equiv b, B$. The quantum corrections at one-loop level were computed using the Passarino-Veltman reduction scheme [58]. This scheme is a fundamental tool for evaluating loop integrals, as it reduces tensor integrals to scalar integrals, known as the scalar Passarino-Veltman functions. The resulting scalar functions are evaluated using Package-X [59,60]. As for the $A_0 \to \gamma\gamma, \gamma Z, ZZ, gg, WW$ decays arising at one-loop level, we have verified that the Feynman diagram contributions are free of ultraviolet divergences.

We find that the generic decay widths of the $A_0 \to \gamma\gamma, \gamma Z, ZZ, gg, WW$ processes at one-loop level are as follows:

$$\Gamma(A_0 \to \gamma\gamma) = \frac{m_{A_0}^3}{256\pi^5}\left|\sum_i m_{f_i} g_{A_0 f_i f_i} g_{\gamma f_i f_i}^2 C_0(0,0,m_{A_0}^2, m_{f_i}^2, m_{f_i}^2, m_{f_i}^2)\right|^2, \tag{8}$$

$$\Gamma(A_0 \to \gamma Z) = \frac{m_{A_0}^3}{128\pi^5}\left(1-\frac{m_Z^2}{m_{A_0}^2}\right)^3\left|\sum_i m_{f_i} g_{A_0 f_i f_i} g_{\gamma f_i f_i} g_V^{Z f_i f_i} C_0(m_{A_0}^2, m_Z^2, 0, m_{f_i}^2, m_{f_i}^2, m_{f_i}^2)\right|^2, \tag{9}$$

$$\begin{aligned}\Gamma(A_0 \to ZZ) = \frac{1}{256\pi^5 m_{A_0}}\left(1-\frac{4m_Z^2}{m_{A_0}^2}\right)^{-1/2}\Bigg|\sum_i m_{f_i} g_{A_0 f_i f_i}[(m_{A_0}^2((g_A^{Z f_i f_i})^2 - (g_V^{Z f_i f_i})^2) + 4m_Z^2 (g_V^{Z f_i f_i})^2) \\ \times C_0(m_{A_0}^2, m_Z^2, m_Z^2, m_{f_i}^2, m_{f_i}^2, m_{f_i}^2) + 4(g_A^{Z f_i f_i})^2 (B_0(m_{A_0}^2, m_{f_i}^2, m_{f_i}^2) - B_0(m_Z^2, m_{f_i}^2, m_{f_i}^2))]\Bigg|^2,\end{aligned} \tag{10}$$

$$\Gamma(A_0 \to gg) = \frac{g_s^4 m_{A_0}^3}{128\pi^5}\left|\sum_i m_{f_i} g_{A_0 f_i f_i} C_0(0,0,m_{A_0}^2, m_{f_i}^2, m_{f_i}^2, m_{f_i}^2)\right|^2, \tag{11}$$

$$\begin{aligned}\Gamma(A_0 \to WW) = \frac{g^4}{512\pi^5 m_{A_0}}\left(1-\frac{4m_W^2}{m_{A_0}^2}\right)^{-1/2}\Bigg|\sum_{i,j} m_{f_i} g_{A_0 f_i f_i}((-m_{f_i}^2 + m_{b_j}^2 + m_W^2) C_0(m_{A_0}^2, m_W^2, m_W^2, m_{f_i}^2, m_{f_i}^2, m_{b_j}^2) \\ + B_0(m_{A_0}^2, m_{f_i}^2, m_{f_i}^2) - B_0(m_W^2, m_{b_j}^2, m_{f_i}^2)) \\ + \sum_{i,j} m_{b_j} g_{A_0 b_j b_j}((-m_{b_j}^2 + m_{f_i}^2 + m_W^2) C_0(m_{A_0}^2, m_W^2, m_W^2, m_{b_j}^2, m_{b_j}^2, m_{f_i}^2) \\ + B_0(m_{A_0}^2, m_{b_j}^2, m_{b_j}^2) - B_0(m_W^2, m_{f_i}^2, m_{b_j}^2))\Bigg|^2.\end{aligned} \tag{12}$$

In Eqs. (8)–(12), the scalar Passarino-Veltman functions are represented by $C_0(0,0,m^2_{A_0},m^2_{f_j},m^2_{f_i},m^2_{f_i})$, $C_0(m^2_{A_0},m^2_Z,0,m^2_{f_i},m^2_{f_i},m^2_{f_i})$, $C_0(m^2_{A_0},m^2_Z,m^2_Z,m^2_{f_i},m^2_{f_i},m^2_{f_i})$, $C_0(m^2_{A_0},m^2_W,m^2_W,m^2_{f_i},m^2_{f_i},m^2_{b_j})$, $B_0(m^2_{A_0},m^2_{f_i},m^2_{f_i})$, $B_0(m^2_Z,m^2_{f_i},m^2_{f_i})$, $B_0(m^2_W,m^2_{b_j},m^2_{f_i})$, $B_0(m^2_{A_0},m^2_{b_j},m^2_{b_j})$, and $B_0(m^2_W,m^2_{f_i},m^2_{b_j})$. On the other hand, the effective couplings ($g_{\gamma f_i f_i}$, $g_{A_0 f_i f_i}$, $g_{A_0 b_j b_j}$, $g_A^{Zf_if_i}$, and $g_V^{Zf_if_i}$) are explicitly provided in the Appendix.

III. NUMERICAL RESULTS

In this section, we present the results for the decay widths and branching ratios of the $A_0 \to b\bar{b}$, $t\bar{t}$, γtt, $\gamma b\bar{b}$, Ztt, Zbb, Wtb, h_0tt, h_0bb, WW, gg, ZZ, $\gamma\gamma$, γZ processes. We also present our numerical analysis for the production via gluon fusion of the pseudoscalar A_0 at current and future colliders within the BLHM framework.

The BLHM parameters involved in our calculation are m_{A_0}, $\tan\beta$, and f. In this way, to establish a benchmark scenario, the pseudoscalar production cross section was calculated by setting the pseudoscalar mass to $m_{A_0} = 500$ GeV [21,23,61,62]. Given the value of m_{A_0}, we can determine the allowed range of values for the parameter $\tan\beta$ (the ratio of the vacuum expectation values of the two Higgs doublets), which is defined by the following equation [13,15]:

$$1 < \tan\beta < \sqrt{\frac{2+2\sqrt{\left(1-\frac{m^2_{h_0}}{m^2_{A_0}}\right)\left(1-\frac{m^2_{h_0}}{4\pi v^2}\right)}}{\frac{m^2_{h_0}}{m^2_{A_0}}\left(1+\frac{m^2_{A_0}-m^2_{h_0}}{4\pi v^2}\right)}-1}. \quad (13)$$

With respect to the energy scale f, this parameter characterizes the scale of new physics and plays a central role in the generation of the masses of the new heavy quarks. Constraints on f arise both from theoretical considerations, such as avoiding excessive fine-tuning in the heavy quark sector, and from experimental bounds on the production of these quarks: $f \in [1\,000, 2\,000]$ GeV [13–15,17]. An additional set of parameters involved in our analysis are the Yukawa couplings y_i ($i = 1, 2, 3$), which are assigned the values $y_1 = 0.61$, $y_2 = 0.84$, and $y_3 = 0.35$ [16,17,52,53].

We first investigate how variations in the parameters f, β or m_{A_0} affect the decay width of the $A_0 \to X$ ($X \equiv t\bar{t}$, $b\bar{b}$, γtt, γbb, Ztt, Zbb, Wtb, h_0tt, h_0bb, WW, gg, ZZ, $\gamma\gamma$, γZ) processes. In Fig. 4(a), we illustrate the behavior of the decay width $\Gamma(A_0 \to X)$ as a function of the scale f while keeping m_{A_0} and $\tan\beta$ fixed. From this figure, we observe that the largest contributions to $\Gamma(A_0 \to X)$ arise from the two-body and three-body tree-level pseudoscalar decays $\Gamma(A_0 \to t\bar{t})$ and $\Gamma(A_0 \to \gamma t\bar{t})$, which represent the dominant and subdominant contributions, respectively, throughout the entire energy interval of the f scale analysis: $\Gamma(A_0 \to t\bar{t}) = [1.26, 1.42]$ GeV and $\Gamma(A_0 \to \gamma t\bar{t}) = [1.39, 1.56] \times 10^{-1}$ GeV. In contrast, the $A_0 \to h_0 b\bar{b}$ decay provides the smallest contribution, i.e., $\Gamma(A_0 \to h_0 b\bar{b}) = [8.34, 8.21] \times 10^{-9}$ GeV while $f \in [1\,000, 2\,000]$ GeV. It is important to note that $A_0 \to X$ decays arising at one-loop level generate numerical contributions of the order of 10^{-4}–10^{-7} GeV. On the other hand, Fig. 4(b) shows our analysis of the impact of the β parameter on $\Gamma(A_0 \to X)$, with the f energy scale fixed at 1 000 GeV and m_{A_0} at 500 GeV. In this scenario, the curves that generate the largest contributions to the decay width $\Gamma(A_0 \to X)$ are again given by the tree-level pseudoscalar decays $A_0 \to t\bar{t}$ and $A_0 \to \gamma t\bar{t}$: $\Gamma(A_0 \to t\bar{t}) = [6.70, 3.39 \times 10^{-1}]$ GeV and $\Gamma(A_0 \to \gamma t\bar{t}) = [7.36 \times 10^{-1}, 3.72 \times 10^{-2}]$ GeV when $\beta \in [\tan^{-1}(1), \tan^{-1}(6)]$ rad. Additionally, the $A_0 \to h_0 b\bar{b}$ decay provides the most suppressed contribution, $\Gamma(A_0 \to h_0 b\bar{b}) = [7.57 \times 10^{-8}, 2.03 \times 10^{-9}]$ GeV. As for the A_0 pseudoscalar decays arising at one-loop level, in this context, the processes generate contributions of the order of 10^{-3} to 10^{-7} GeV, these contributions are slightly larger compared to those obtained in the $\Gamma(A_0 \to X)$ vs f analysis scenario. In the two previous scenarios, the generated curves were obtained for a fixed value of m_{A_0}. In Fig. 4(c), we instead analyze the behavior of $\Gamma(A_0 \to X)$ as a function of the pseudoscalar mass m_{A_0}, varying this free parameter in the range of 500 to 2 000 GeV while keeping the other parameters fixed at $f = 1\,000$ GeV and $\tan\beta = 3$. In this figure, most of the curves exhibit an increasing trend within the analyzed m_{A_0} interval. We also observe that the decays $A_0 \to t\bar{t}$ and $A_0 \to \gamma t\bar{t}$ continue to provide the dominant and subdominant numerical contributions, with the corresponding decay widths of $\Gamma(A_0 \to t\bar{t}) = [1.26, 6.87]$ GeV and $\Gamma(A_0 \to \gamma t\bar{t}) = [1.39, 7.65] \times 10^{-1}$ GeV, respectively. As can be clearly seen in Figs. 4(b) and 4(c), the curves of $\Gamma(A_0 \to X)$ as a function of β and as a function of m_{A_0} exhibits appreciable variations within the respective analysis intervals defined for β and m_{A_0}. This leads us to conclude that $\Gamma(A_0 \to X)$ shows a strong dependence on these two parameters. In contrast, $\Gamma(A_0 \to X)$ shows little sensitivity to changes in f scale values; the corresponding curves decrease slightly as f increases.

Figure 5 shows the corresponding branching ratios $\mathrm{Br}(A_0 \to X)$ for the $A_0 \to X$ decays. The total decay width (Γ_{A_0}) of the pseudoscalar Higgs boson A_0 has been calculated taking into account the following pseudoscalar decay modes: $t\bar{t}$, $b\bar{b}$, γtt, γbb, Ztt, Zbb, Wtb, h_0tt, h_0bb, WW, gg, ZZ, $\gamma\gamma$, γZ. In Fig. 5(a), the dependence of $\mathrm{Br}(A_0 \to X)$ vs f is analyzed. In this plot, we see that the most probable decay channels of the pseudoscalar are given by the $A_0 \to t\bar{t}$ and $A_0 \to \gamma t\bar{t}$ processes when $f \in [1\,000, 2\,000]$ GeV. These decays arise at tree level and generate dominant and subdominant contributions to $\mathrm{Br}(A_0 \to X)$: $\mathrm{Br}(A_0 \to t\bar{t}) \approx 8.92 \times 10^{-1}$ and

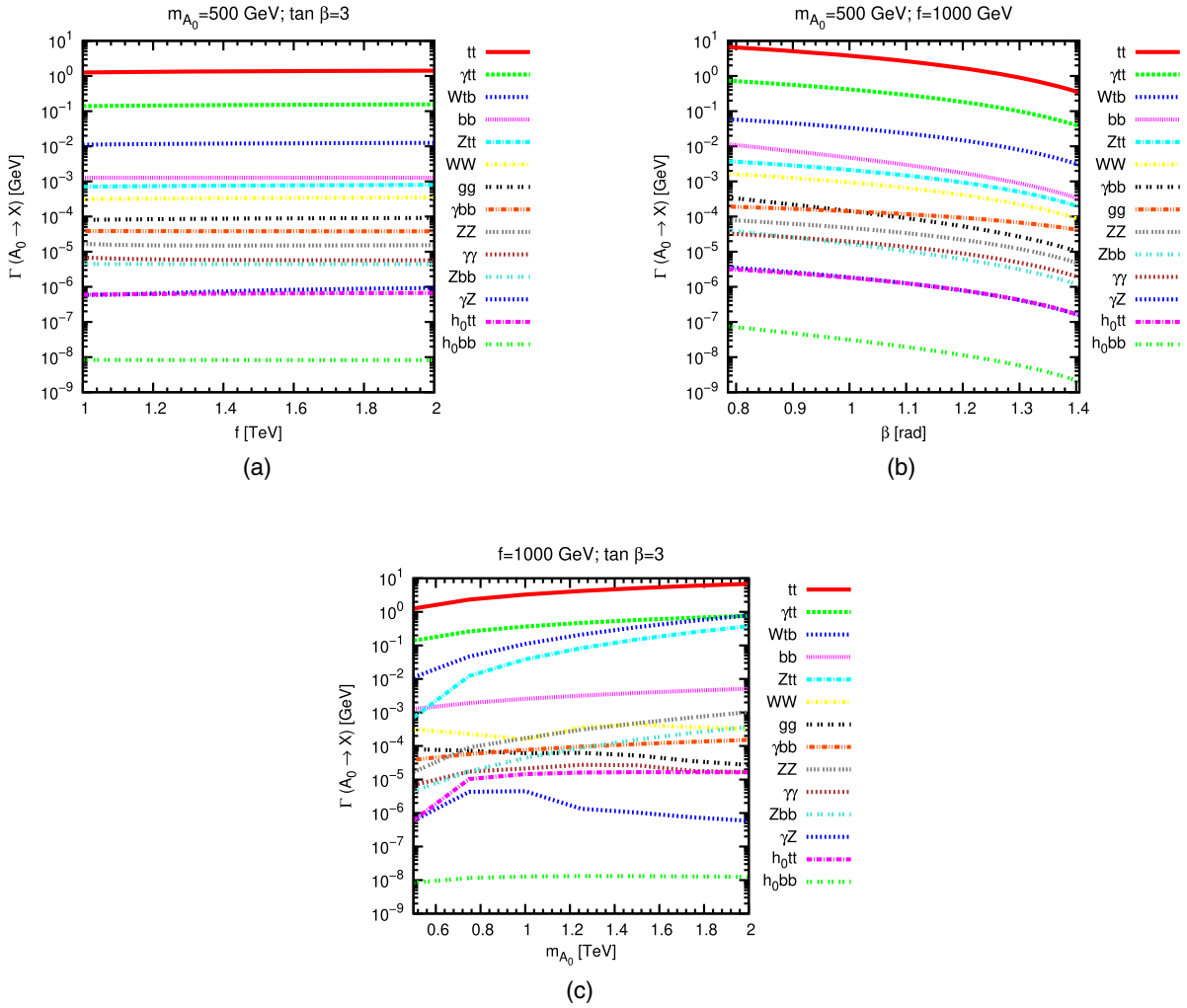


FIG. 4. Decay widths for the $A_0 \to X$ processes where $X \equiv t\bar{t}$, $b\bar{b}$, γtt, γbb, Ztt, Zbb, Wtb, h_0tt, h_0bb, WW, gg, ZZ, $\gamma\gamma$, γZ. (a) $\Gamma(A_0 \to X)$ as a function of the f energy scale. (b) $\Gamma(A_0 \to X)$ as a function of the parameter β ($\tan\beta \in [1, 6]$). (c) $\Gamma(A_0 \to X)$ as a function of the mass of the pseudoscalar A_0.

$\mathrm{Br}(A_0 \to \gamma t\bar{t}) \approx 9.81 \times 10^{-2}$, respectively. While the numerical values do not show a strong sensitivity of $\mathrm{Br}(A_0 \to X)$ to f at first glance, a variation becomes noticeable after a few digits beyond the decimal point. On the other hand, it is observed that the $A_0 \to h_0 b\bar{b}$ decay generates the smallest contribution to the branching ratio, that is, $\mathrm{Br}(A_0 \to h_0 b\bar{b}) = [5.90, 5.17] \times 10^{-9}$. Regarding the plot in Fig. 5(b), in this scenario, we generate curves by varying the β parameter while the other parameters remain unchanged, i.e., $m_{A_0} = 500$ GeV and $f = 1\,000$ GeV. In the corresponding figure, we see that the two main contributions are $\mathrm{Br}(A_0 \to t\bar{t}) \approx 8.92 \times 10^{-1}$ and $\mathrm{Br}(A_0 \to \gamma t\bar{t}) = [9.80, 9.81] \times 10^{-2}$ when $\beta \in [\tan^{-1}(1), \tan^{-1}(6)]$ rad. On the contrary, the most suppressed contribution comes from $A_0 \to h_0 b\bar{b}$ decay, which gives branching ratios of $\mathrm{Br}(A_0 \to h_0 b\bar{b}) = [1.01 \times 10^{-8}, 5.35 \times 10^{-9}]$ in the study interval for the β parameter. Regarding the curves generated in the analysis of $\mathrm{Br}(A_0 \to X)$ vs m_{A_0}, as shown in Fig. 5(c), the decay channels $A_0 \to t\bar{t}$ and $A_0 \to \gamma t\bar{t}$ provide the highest probabilities for the particle A_0 to decay into these specific channels. The numerical contributions for the aforementioned processes are $\mathrm{Br}(A_0 \to t\bar{t}) = [8.92, 7.80] \times 10^{-1}$ and $\mathrm{Br}(A_0 \to \gamma t\bar{t}) = [9.81, 8.68] \times 10^{-2}$ while $m_{A_0} \in [500, 2\,000]$ GeV. Notably, in the three study scenarios ($\mathrm{Br}(A_0 \to X)$ vs f, $\mathrm{Br}(A_0 \to X)$ vs β, and $\mathrm{Br}(A_0 \to X)$ vs m_{A_0}), the one-loop $A_0 \to X$ decays produce branching ratios on the order of 10^{-4} to 10^{-7}. $\mathrm{Br}(A_0 \to X)$ shows greater dependence on the m_{A_0} parameter; the effects are quite noticeable in the curves [see Fig. 5(c)].

A. Production cross section of the pseudoscalar A_0 at the LHC and FCC-hh

In this subsection, we present the Breit-Wigner resonance formula, which is useful for describing the resonant production of the pseudoscalar Higgs boson A_0. Although

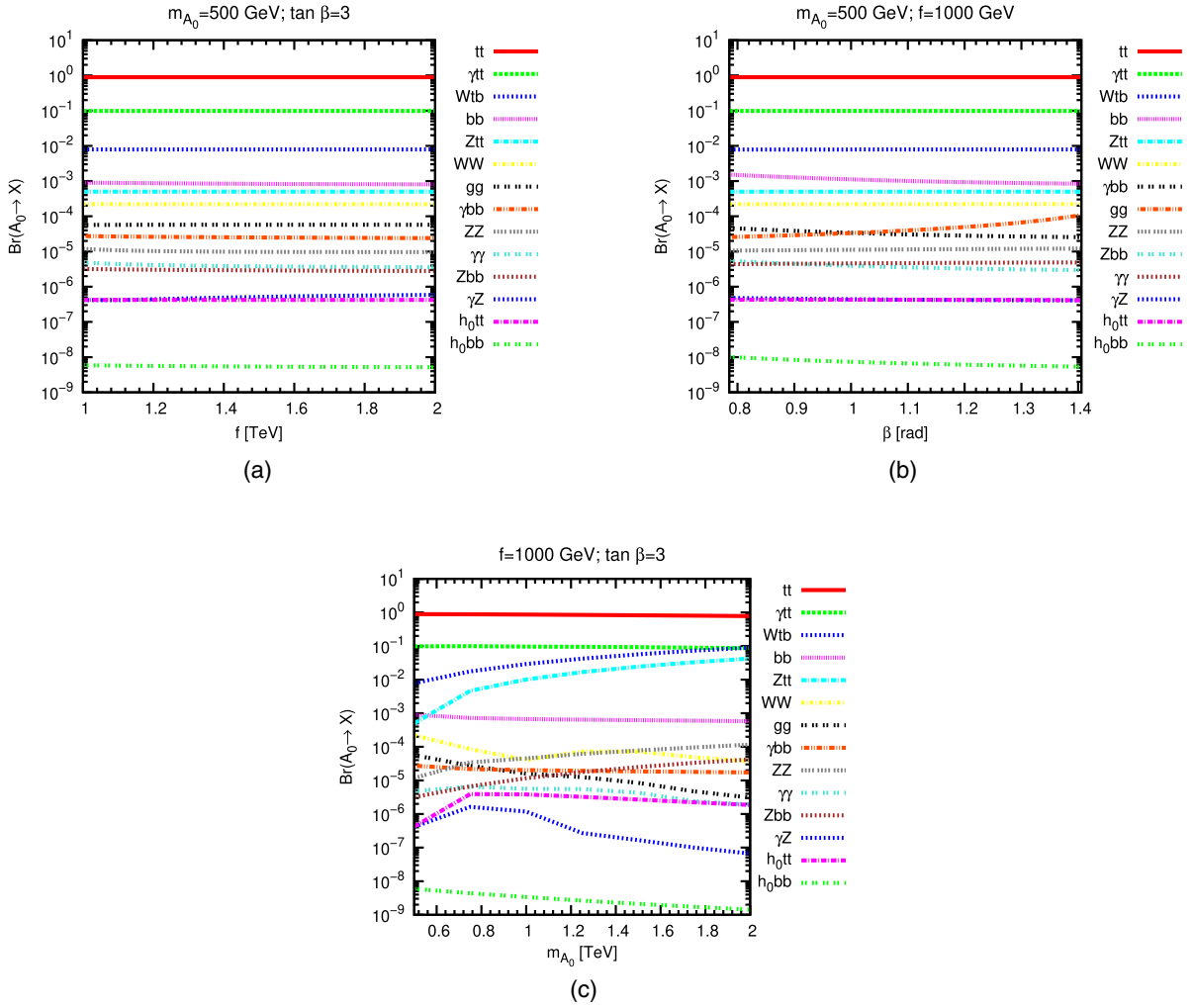


FIG. 5. Branching ratios for the $A_0 \to X$ processes where $X \equiv t\bar{t}$, $b\bar{b}$, γtt, γbb, Ztt, Zbb, Wtb, h_0tt, h_0bb, WW, gg, ZZ, $\gamma\gamma$, γZ. (a) $\mathrm{Br}(A_0 \to X)$ as a function of the f energy scale. (b) $\mathrm{Br}(A_0 \to X)$ as a function of the parameter β ($\tan\beta \in [1, 6]$). (c) $\mathrm{Br}(A_0 \to X)$ as a function of the mass of the pseudoscalar A_0.

Eq. (14) is determined just at the resonance of the pseudoscalar, it provides an approximate description of the pseudoscalar production mechanism via gluon fusion in the BLHM, it can also serve as a theoretical reference for guiding experimental searches for this new particle. It is worth stressing that the Breit-Wigner formula is valid under the conditions that the decay width of the resonance is small compared to its mass, and that the machine's energy spread is much smaller than the physical width of the intermediate particle, such as the pseudoscalar A_0. These assumptions have been taken into account in our study. Otherwise, the Breit-Wigner expression must be corrected by convoluting it with the actual beam energy spectrum. Under this approximation, the production cross section of A_0 via gluon fusion can be expressed as follows [55]:

$$\sigma(gg \to A_0 \to Y) = \frac{\pi}{36} \frac{\Gamma(A_0 \to gg)\Gamma(A_0 \to Y)}{m_{A_0}^2 \Gamma_{A_0}^2}, \quad (14)$$

where $\Gamma(A_0 \to gg)$ and $\Gamma(A_0 \to Y)$ (with $Y \equiv t\bar{t}, b\bar{b}, \gamma\gamma, \gamma Z, ZZ, gg, WW$) are the partial decay widths for an on-shell A_0 to decay to the initial and final states, respectively.

Using Eq. (14), we generated the curves shown in Fig. 6 for $m_{A_0} = 500$ GeV, in which we studied the behavior of the cross section $\sigma(gg \to A_0 \to Y)$ as a function of parameter f or β, while fixing the other model parameters. We first discuss the behavior observed in Fig. 6(a) when $\tan\beta = 3.0$. Note that the magnitude of $\sigma(gg \to A_0 \to Y)$ depends slightly on the f energy scale, except for the $gg \to A_0 \to \gamma Z$ decay channel, which gives a curve with more appreciable changes within the range of study of the f parameter, $f \in [1\,000, 2\,000]$ GeV. In the same context, we find that the $gg \to A_0 \to t\bar{t}$ and $gg \to A_0 \to \gamma Z$ decay channels generate the largest and smallest cross sections over the entire f interval: $\sigma(gg \to A_0 \to t\bar{t}) = [6.87, 6.97]$ fb and $\sigma(gg \to A_0 \to \gamma Z) = [3.21, 4.57] \times 10^{-6}$ fb. Regarding Fig. 6(b), this plot shows the results for the pseudoscalar production cross section when the f scale is fixed at $f = 1\,000$ GeV, and the β parameter

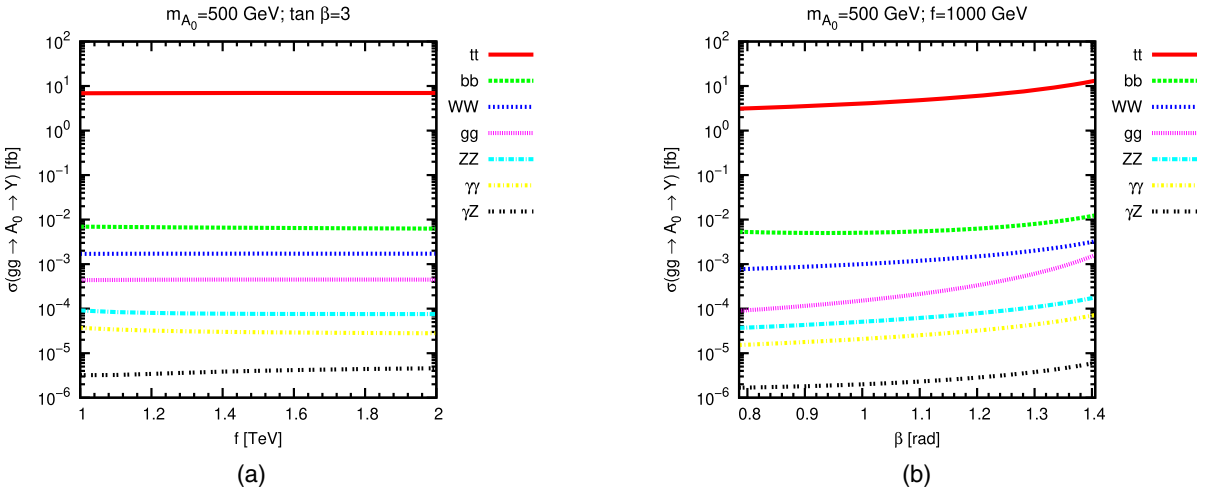


FIG. 6. Production cross section of the pseudoscalar A_0 (for $m_{A_0} = 500$ GeV) via gluon fusion. (a) $\sigma(gg \to A_0 \to Y)$ as a function of the f energy scale. (b) $\sigma(gg \to A_0 \to Y)$ as a function of the parameter β ($\tan\beta \in [1, 6]$).

varies within the range $\tan^{-1}(1)$ to $\tan^{-1}(6)$ rad. Once again, the $gg \to A_0 \to t\bar{t}$ process gives the largest contribution to $\sigma(gg \to A_0 \to Y)$, while the $gg \to A_0 \to \gamma Z$ decay channel yields the most suppressed contribution, i.e., $\sigma(gg \to A_0 \to t\bar{t}) = [3.11, 13.15]$ fb and $\sigma(gg \to A_0 \to \gamma Z) = [1.68, 6.06] \times 10^{-6}$ fb. The various curves obtained in the analysis of the $\sigma(gg \to A_0 \to Y)$ production cross section as a function of β exhibit a growth of up to two orders of magnitude as β increases toward 1.4 rad, as shown in the Fig. 6(b). It is evident that the region with the greater predictive importance corresponds to values of β around 1.4 rad.

We now turn to discuss the dependence of $\sigma(gg \to A_0 \to Y)$ on the m_{A_0} parameter when it varies from 500 to 2 000 GeV, as depicted in Fig. 7. In this figure, the curves have been generated for the values of $f = 1\,000$ GeV and $\tan\beta = 3$, as well as $f = 2\,000$ GeV and $\tan\beta = 6$. In the first scenario [see Fig. 7(a)], numerical evaluation shows that the $gg \to A_0 \to t\bar{t}$ decay channel provides the largest cross section while $m_{A_0} \in [500, 2\,000]$ GeV: $\sigma(gg \to A_0 \to t\bar{t}) = [6.87, 2.05 \times 10^{-2}]$ fb. With respect to the second scenario [see Fig. 7(b)], again the $gg \to A_0 \to t\bar{t}$ decay generate the largest contribution to $\sigma(gg \to A_0 \to Y)$, i.e., $\sigma(gg \to A_0 \to t\bar{t}) = [13.41, 2.73 \times 10^{-2}]$ fb. In both study scenarios, we observe that the pseudoscalar production cross section decreases as the mass of A_0 increases. It is also evident that $\sigma(gg \to A_0 \to Y)$ strongly depends on the m_{A_0} parameter. In general, the $gg \to A_0 \to \gamma Z$ decay channel provides the smallest numerical contributions to $\sigma(gg \to A_0 \to Y)$. It is important to note that the production cross sections of the $A_0 \to VV$ processes, which arise at the one-loop level, yield significantly more suppressed numerical values than those of the fermionic decay channels that occur at tree level.

In the experimental context, the production mechanism of the pseudoscalar A_0 via gluon fusion could be studied at the LHC, particularly in its future upgrades such as the

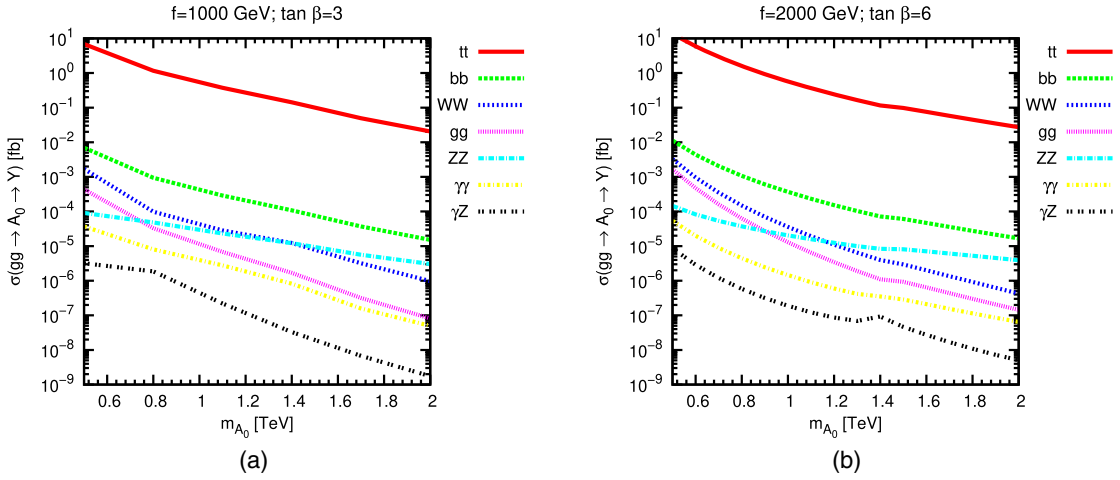


FIG. 7. Production cross section of the pseudoscalar A_0 via gluon fusion as a function of the parameter m_{A_0}: (a) $f = 1\,000$ GeV and $\tan\beta = 3$, and (b) $f = 2\,000$ GeV and $\tan\beta = 6$.

high-luminosity LHC (HL-LHC) and the high-energy LHC (HE-LHC), as well as in future high-energy colliders like the FCC-hh. The HL-LHC [36–39] is planned to operate at a center-of-mass energy of 14 TeV with an integrated luminosity of 3 000 fb^{-1}, while the HE-LHC [36–39] would provide proton-proton collisions at a center-of-mass energy of 27 TeV with an integrated luminosity of 10 000 fb^{-1}. Accurate exploration of rare processes will be made possible by the LHC upgrades, which promise to increase the collision energy. As for the future hadron collider, the FCC-hh is designed to operate at a center-of-mass energy of $\sqrt{s} = 100$ TeV and to collect a total integrated luminosity of 30 000 fb^{-1} [40–43]. This would allow the exploration of regions of parameter space that are currently inaccessible and would significantly increase the potential to study processes with extremely small cross sections. The FCC-hh is considered one of the most promising projects for the discovery of new particles in the coming decades.

Using the numerical results for the pseudoscalar production cross sections and considering the expected integrated luminosities of the HL-LHC, HE-LHC, and FCC-hh colliders, we can estimate the number of events that could be observed at these colliders for the $A_0 \to Y$ pseudoscalar decays. Tables I–VII present the expected number of events associated with the $A_0 \to Y$ decays when the new physics scale f takes specific values such as 1 000 and 2 000 GeV. It is important to emphasize that these event estimates were generated with $m_{A_0} = 500$ GeV. In this context, we find that the production of the pseudoscalar A_0 through the decay channels $A_0 \to t\bar{t}, b\bar{b}$, and $A_0 \to WW, gg$

TABLE I. The number of expected events related to $A_0 \to t\bar{t}$ decay.

	$m_{A_0} = 500$ GeV, $\tan\beta = 6$		
	No. of expected events at the colliders:		
	HL-LHC	HE-LHC	FCC-hh
f [TeV]	$\mathcal{L} = 3\,000$ fb^{-1}	$\mathcal{L} = 10\,000$ fb^{-1}	$\mathcal{L} = 30\,000$ fb^{-1}
1	37 524	131 749	395 247
2	40 233	134 112	402 336

TABLE II. The number of expected events related to $A_0 \to b\bar{b}$ decay.

	$m_{A_0} = 500$ GeV, $\tan\beta = 6$		
	No. of expected events at the colliders:		
	HL-LHC	HE-LHC	FCC-hh
f [TeV]	$\mathcal{L} = 3\,000$ fb^{-1}	$\mathcal{L} = 10\,000$ fb^{-1}	$\mathcal{L} = 30\,000$ fb^{-1}
1	37	124	373
2	34	112	337

TABLE III. The number of expected events related to $A_0 \to WW$ decay.

	$m_{A_0} = 500$ GeV, $\tan\beta = 6$		
	No. of expected events at the colliders:		
	HL-LHC	HE-LHC	FCC-hh
f [TeV]	$\mathcal{L} = 3\,000$ fb^{-1}	$\mathcal{L} = 10\,000$ fb^{-1}	$\mathcal{L} = 30\,000$ fb^{-1}
1	10	32	98
2	10	33	99

TABLE IV. The number of expected events related to $A_0 \to gg$ decay.

	$m_{A_0} = 500$ GeV, $\tan\beta = 6$		
	No. of expected events at the colliders:		
	HL-LHC	HE-LHC	FCC-hh
f [TeV]	$\mathcal{L} = 3\,000$ fb^{-1}	$\mathcal{L} = 10\,000$ fb^{-1}	$\mathcal{L} = 30\,000$ fb^{-1}
1	5	16	48
2	5	17	50

TABLE V. The number of expected events related to $A_0 \to ZZ$ decay.

	$m_{A_0} = 500$ GeV, $\tan\beta = 6$		
	No. of expected events at the colliders:		
	HL-LHC	HE-LHC	FCC-hh
f [TeV]	$\mathcal{L} = 3\,000$ fb^{-1}	$\mathcal{L} = 10\,000$ fb^{-1}	$\mathcal{L} = 30\,000$ fb^{-1}
1	1	2	5
2	0	1	4

TABLE VI. The number of expected events related to $A_0 \to \gamma\gamma$ decay.

	$m_{A_0} = 500$ GeV, $\tan\beta = 6$		
	No. of expected events at the colliders:		
	HL-LHC	HE-LHC	FCC-hh
f [TeV]	$\mathcal{L} = 3\,000$ fb^{-1}	$\mathcal{L} = 10\,000$ fb^{-1}	$\mathcal{L} = 30\,000$ fb^{-1}
1	0	1	2
2	0	0	2

TABLE VII. The number of expected events related to $A_0 \to \gamma Z$ decay.

	$m_{A_0} = 500$ GeV, $\tan\beta = 6$		
	No. of expected events at the colliders:		
	HL-LHC	HE-LHC	FCC-hh
f [TeV]	$\mathcal{L} = 3\,000$ fb^{-1}	$\mathcal{L} = 10\,000$ fb^{-1}	$\mathcal{L} = 30\,000$ fb^{-1}
1	0	0	0
2	0	0	0

TABLE VIII. The number of expected events at the FCC-hh for the $A_0 \to Y$ decay.

	$m_{A_0} = 1\,000$ GeV, $\tan\beta = 6$				
	No. of expected events at the FCC-hh:				
f [TeV]	$A_0 \to t\bar{t}$ $\mathcal{L} = 30\,000$ fb^{-1}	$A_0 \to b\bar{b}$ $\mathcal{L} = 30\,000$ fb^{-1}	$A_0 \to WW$ $\mathcal{L} = 30\,000$ fb^{-1}	$A_0 \to gg, ZZ$ $\mathcal{L} = 30\,000$ fb^{-1}	$A_0 \to \gamma\gamma, \gamma Z$ $\mathcal{L} = 30\,000$ fb^{-1}
1	27 494	20	1	1	0
2	17 154	11	1	0	0

(see Tables I–IV), which arise at tree level and one-loop level, respectively, provides promising scenarios for the experiments of interest.

Additionally, Table VIII presents the number of events for the production of the pseudoscalar A_0 through the $A_0 \to Y$ decays when $m_{A_0} = 1000$ GeV is selected. Note that, for this reference scenario, the production of the pseudoscalar A_0 via gluon fusion occurs predominantly through the $A_0 \to t\bar{t}$ and $A_0 \to b\bar{b}$ decay channels, while the remaining decay modes are suppressed.

B. The $gg \to t\bar{t} \to WbW\bar{b} \to X_W b\bar{b}$ signal and SM backgrounds

In the present work, our focus has been on providing a first phenomenological exploration of the pseudoscalar A_0 in the BLHM by computing its decay widths, branching ratios, and production cross sections, and by estimating the number of expected events at different collider setups. This represents a important step before undertaking a full collider-level simulation, but rather provides benchmark results that serve as input for future investigations. A realistic study of the $gg \to A_0 \to Y$ processes at the collider-level is planned for future research. In future work, we plan to extend this analysis to include the most relevant SM backgrounds and to explore strategies for enhancing the signal significance. It is also important to note that a collider-level study would require much more time; therefore, this analysis is planned for future research.

In this subsection, we study the production mechanism $gg \to A_0 \to t\bar{t} \to WbW\bar{b} \to X_W b\bar{b}$, where X_W denotes the leptonic $(l^+\nu_l l^-\bar{\nu}_l)$, semileptonic $(l^+\nu_l qq')$, and hadronic $(qq'qq')$ decay channels. This is the dominant signal for A_0 production in the BLHM framework at hadron colliders. We also analyze SM background cross sections. Below, we detail the main processes contributing to both the signal and the SM backgrounds.

Signal:

$$\textbf{Gluon fusion} \quad gg \to A_0 \to t\bar{t} \to WbW\bar{b} \to \begin{cases} l^+\nu_l l^-\bar{\nu}_l b\bar{b} \\ l^+\nu_l qq' b\bar{b} \\ qq'qq' b\bar{b} \end{cases}, \text{ with } \quad l = e, \mu\,.$$

SM Background:

(i) $gg \to t\bar{t}$,
(ii) $gg \to h_0 ZZ$,
(iii) $gg \to h_0 h_0 Z$,
(iv) $gg \to h_0 WW$,
(v) $gg \to WWZ$.

For the analysis, we apply the narrow-width approximation to simplify calculations. This method yields the total cross section of the $\sigma(gg \to A_0 \to t\bar{t} \to WbW\bar{b} \to X_W b\bar{b})$ signal,

$$\begin{aligned} &\sigma(gg \to A_0 \to t\bar{t} \to WbW\bar{b} \to X_W b\bar{b}) \\ &\simeq \sigma(gg \to A_0 \to t\bar{t}) \times \mathrm{Br}(t \to Wb) \\ &\quad \times \mathrm{Br}(\bar{t} \to W\bar{b})\mathrm{Br}(W)\mathrm{Br}(W), \end{aligned} \tag{15}$$

where $\mathrm{Br}(W)$ is the branching ratio of the W bosons in our process. We consider that the W boson decays leptonic, semileptonic, or hadronic for the signal. Table IX shows representative cross sections for the SM backgrounds of the $gg \to A_0 \to t\bar{t} \to WbW\bar{b} \to X_W b\bar{b}$ signal at the HL-LHC, HE-LHC, and the FCC-hh.

In Table X lists the cross sections for the $gg \to A_0 \to t\bar{t} \to WbW\bar{b} \to X_W b\bar{b}$ signal and dominant background processes $(gg \to h_0 h_0 Z/WWZ/t\bar{t})$ in hadron colliders. The parameters are $m_{A_0} = 500$ GeV, $f = 1000$ GeV, and $\tan\beta = 6$.

Complementarily, in Table XI, we present the number of expected events for the signal $gg \to A_0 \to t\bar{t} \to WbW\bar{b} \to X_W b\bar{b}$, where we have considered the dominant SM background processes: $gg \to t\bar{t}$, $gg \to h_0 h_0 Z$, and $gg \to WWZ$. Table XI shows that producing the pseudoscalar Higgs boson A_0 of the BLHM at the HL-LHC, HE-LHC, and FCC-hh via $gg \to A_0 \to t\bar{t} \to WbW\bar{b} \to X_W b\bar{b}$

TABLE IX. Representative cross sections for the SM background processes of the $gg \to A_0 \to t\bar{t} \to WbW\bar{b} \to X_W b\bar{b}$ signal at the hadron colliders for the center-of-mass energies of $\sqrt{s} = 14$, 27, 100 TeV.

Background cross section [fb]			
Process	$\sqrt{s} = 14$ TeV (HL-LHC)	$\sqrt{s} = 27$ TeV (HE-LHC)	$\sqrt{s} = 100$ TeV (FCC-hh)
$gg \to t\bar{t}$	1.03	1.02	1.01
$gg \to h_0 h_0 Z$	4 916.56	67 413.40	1.26×10^7
$gg \to WWZ$	295.23	1 085.49	14 800.10
$gg \to h_0 ZZ$	2.60×10^{-1}	4.37×10^{-1}	1.05
$gg \to h_0 WW$	2.54×10^{-1}	4.28×10^{-1}	1.03

TABLE X. Representative cross sections for $gg \to A_0 \to t\bar{t} \to WbW\bar{b} \to X_W b\bar{b}$ signal and dominant backgrounds ($gg \to h_0 h_0 Z/WWZ/t\bar{t}$) are given for hadron colliders at center-of-mass energies $\sqrt{s} = 14$, 27, and 100 TeV. The different decay channels of $W^{\pm}$ bosons are considered.

$m_{A_0} = 500$ GeV, $f = 1000$ GeV, $\tan\beta = 6$		
Signal cross section [fb]: $\sigma(gg \to A_0 \to t\bar{t} \to WbW\bar{b} \to qq'qq'b\bar{b})$		
$\sqrt{s} = 14$ TeV (HL-LHC)	$\sqrt{s} = 27$ TeV (HE-LHC)	$\sqrt{s} = 100$ TeV (FCC-hh)
2 172.50	28 510.90	5.26×10^6
Signal cross section [fb]: $\sigma(gg \to A_0 \to t\bar{t} \to WbW\bar{b} \to l^+\nu_l qq'b\bar{b})$		
$\sqrt{s} = 14$ TeV (HL-LHC)	$\sqrt{s} = 27$ TeV (HE-LHC)	$\sqrt{s} = 100$ TeV (FCC-hh)
349.99	4 593.22	847 241.12
Signal cross section [fb]: $\sigma(gg \to A_0 \to t\bar{t} \to WbW\bar{b} \to l^+\nu_l l^-\bar{\nu}_l b\bar{b})$		
$\sqrt{s} = 14$ TeV (HL-LHC)	$\sqrt{s} = 27$ TeV (HE-LHC)	$\sqrt{s} = 100$ TeV (FCC-hh)
56.39	739.98	136 494.01

is an effective way to study this particle. This production channel may represent a promising scenario.

C. The $gg \to WW \to X_W$ signal and SM backgrounds

We will proceed with the analysis of the production mechanism $gg \to A_0 \to WW \to X_W$. This process represents the dominant signal for the production of the pseudoscalar A_0 when it decays into a pair of vector bosons. We also analyze dominant SM background processes. We then describe the signal and SM backgrounds of the aforementioned process.

Signal:

$$\textbf{Gluon fusion} \quad gg \to A_0 \to W^+W^- \to \begin{cases} l^+\nu_l l^-\bar{\nu}_l \\ l^+\nu_l qq' \\ qq'qq' \end{cases}, \text{ with } \quad l = e, \mu\,.$$

SM background:

(i) $gg \to WW$,
(ii) $gg \to ZZ$,
(iii) $gg \to Z\gamma$.

As in the previous subsection, we use the narrow-width approximation to determine the total cross section of the $gg \to A_0 \to W^+W^- \to X_W$ signal, which leads to the following expression

$$\sigma(gg \to A_0 \to W^+W^- \to X_W) \simeq \sigma(gg \to A_0 \to W^+W^-) \times \mathrm{Br}(W^+) \times \mathrm{Br}(W^-), \quad (16)$$

with $\mathrm{Br}(W^{\pm})$, the branching ratio of the vector boson $W^{\pm}$.

The cross sections for the SM background processes of the $gg \to A_0 \to W^+W^- \to X_W$ signal at the LHC and the FCC-hh are shown below (see Table XII).

TABLE XI. Total production of $gg \to A_0 \to t\bar{t} \to WbW\bar{b} \to X_W b\bar{b}$ and dominant backgrounds ($gg \to h_0 h_0 Z/WWZ/t\bar{t}$) at hadron colliders in the BLHM context. Values are for $m_{A_0} = 500$ GeV, $f = 1000$ GeV, and $\tan\beta = 6$. Leptonic, semileptonic, and hadronic $W^{\pm}W^{\mp}$ final states are considered.

$m_{A_0} = 500$ GeV				
	$f = 1\,000$ GeV, $\tan\beta = 6$			
$\mathcal{L}$ (fb^{-1})	$\sqrt{s}$ [TeV]	Leptonic channel	Semileptonic channel	Hadronic channel
3000	14	169 158	1.05×10^6	6.52×10^6
10 000	27	7.39×10^6	4.59×10^7	2.85×10^8
30 000	100	4.09×10^9	2.54×10^{10}	1.57×10^{11}

TABLE XII. Representative cross sections for the background of the $gg \to A_0 \to W^+W^- \to X_W$ signal at the hadron colliders for the center-of-mass energies of $\sqrt{s} = 14$, 27, 100 TeV.

Background cross section [fb]			
Process	$\sqrt{s} = 14$ TeV (HL-LHC)	$\sqrt{s} = 27$ TeV (HE-LHC)	$\sqrt{s} = 100$ TeV (FCC-hh)
$gg \to WW$	9.29×10^{-2}	4.18×10^{-2}	7.29×10^{-3}
$gg \to ZZ$	4.69×10^{-2}	2.11×10^{-2}	3.68×10^{-3}
$gg \to \gamma Z$	5.49×10^{-14}	3.97×10^{-15}	2.11×10^{-17}

TABLE XIII. Representative cross sections for the $gg \to A_0 \to W^+W^- \to X_W$ signal and dominant backgrounds ($gg \to WW/ZZ$) at the hadron colliders for the center-of-mass energies of $\sqrt{s} = 14$, 27, 100 TeV. The different decay channels of $W^{\pm}$ bosons are considered.

$m_{A_0} = 500$ GeV, $f = 1000$ GeV, $\tan\beta = 6$		
Signal cross section [fb]: $\sigma(gg \to A_0 \to W^+W^- \to l^+\nu_l l^-\bar{\nu}_l)$		
$\sqrt{s} = 14$ TeV (HL-LHC)	$\sqrt{s} = 27$ TeV (HE-LHC)	$\sqrt{s} = 100$ TeV (FCC-hh)
1.67×10^{-3}	7.64×10^{-4}	1.52×10^{-4}
Signal cross section [fb]: $\sigma(gg \to A_0 \to W^+W^- \to l^+\nu_l qq')$		
$\sqrt{s} = 14$ TeV (HL-LHC)	$\sqrt{s} = 27$ TeV (HE-LHC)	$\sqrt{s} = 100$ TeV (FCC-hh)
1.04×10^{-2}	4.74×10^{-3}	9.45×10^{-4}
Signal cross section [fb]: $\sigma(gg \to A_0 \to W^+W^- \to qq'qq')$		
$\sqrt{s} = 14$ TeV (HL-LHC)	$\sqrt{s} = 27$ TeV (HE-LHC)	$\sqrt{s} = 100$ TeV (FCC-hh)
6.44×10^{-2}	2.94×10^{-2}	5.87×10^{-3}

TABLE XIV. The total production of $gg \to A_0 \to W^+W^- \to X_W$ and dominant backgrounds ($gg \to WW/ZZ$) at the hadron colliders in the context of the BLHM when $m_{A_0} = 500$ GeV with $f = 1\,000$ GeV and $\tan\beta = 6$. The leptonic, semileptonic, and hadronic channels of the $W^{\pm}W^{\mp}$ in the final state are considered.

$m_{A_0} = 500$ GeV				
	$f = 1\,000$ GeV, $\tan\beta = 6$			
$\mathcal{L}$ (fb^{-1})	$\sqrt{s}$ [TeV]	Leptonic channel	Semileptonic channel	Hadronic channel
3000	14	5	31	193
10 000	27	7	47	294
30 000	100	5	28	176

In Table XIII, we present the numerical values generated for the cross sections of the $gg \to A_0 \to W^+W^- \to X_W$ signal and dominant SM backgrounds ($gg \to WW/ZZ$) in hadron colliders when $m_{A_0} = 500$ GeV, $f = 1\,000$ GeV, and $\tan\beta = 6$.

We present the expected number of events for the signal process $gg \to A_0 \to W^+W^- \to X_W$, taking into account the dominant SM background processes $gg \to WW$ and $gg \to ZZ$, as summarized in Table XIV.

The results presented in Table XIV show that the total production of the pseudoscalar Higgs boson A_0 in the BLHM at the LHC and the FCC-hh through the signal process $gg \to A_0 \to W^+W^- \to X_W$ leads to a suppressed and relatively unpromising scenario when compared to the production of A_0 via the $gg \to A_0 \to t\bar{t} \to WbW\bar{b} \to X_W b\bar{b}$ signal.

IV. CONCLUSIONS

Within the BLHM framework, we investigate the production of the pseudoscalar A_0 through gluon fusion at future colliders, such as the HL-LHC, HE-LHC, and FCC-hh. These experiments promise to extend current searches for heavy particles, such as the pseudoscalar of interest to us.

In our study of the pseudoscalar A_0, we analyze the impact of the free parameters of the BLHM (f, β, and m_{A_0}) on the partial decay widths and branching ratios of the pseudoscalar, considering both two-and three-body decays at tree level, as well as one-loop level decays. For the one-loop decays, we account for the virtual particle effects induced by both the BLHM and SM particles. We also investigate the resonant production of the pseudoscalar A_0 using the Breit-Wigner resonance formula, evaluated specifically at the resonance peak of the pseudoscalar. Within this approach, we examine the sensitivity of the $\sigma(gg \to A_0 \to Y)$ production cross section to the parameters f, β, and m_{A_0}, considering the following study intervals: $f \in [1\,000, 2\,000]$ GeV, $\beta \in [\tan^{-1}(1), \tan^{-1}(6)]$ radians, and $m_{A_0} \in [500, 2\,000]$ GeV. Our numerical results show that $\sigma(gg \to A_0 \to Y)$ increases by up to two orders of magnitude as β approaches 1.4 radians, indicating a strong dependence on this parameter. We find that the region of highest predictive significance corresponds to values of β around approximately 1.4 radians. Additionally, we observe that the pseudoscalar production cross section decreases as the mass m_{A_0} increases.

To establish a benchmark, Tables I–VIII present the expected number of events from the production of the pseudoscalar for two different mass values: $m_{A_0} = 500$ GeV and $m_{A_0} = 1\,000$ GeV. To estimate the number of events that could be observed at the colliders for the pseudoscalar decays $A_0 \to Y$, we have considered the expected integrated luminosities of the HL-LHC, HE-LHC, and FCC-hh. In the first scenario, when $m_{A_0} = 500$ GeV, we find that the production of the pseudoscalar A_0 through the $A_0 \to t\bar{t}$ and $A_0 \to b\bar{b}$ decay channels (see Tables I and II), which arise at tree level, provide very promising scenarios for the experiments of interest. In the second scenario, when $m_{A_0} = 1\,000$ GeV, the most abundant production of the pseudoscalar is associated with the fermionic $A_0 \to t\bar{t}$ channel at the FCC-hh, while the other decay channels are suppressed. According to the numerical results (figures and tables), we find that the region with the highest predictive significance for the potential discovery of the pseudoscalar A_0 corresponds to values of m_{A_0} around 500 GeV and to β at approximately $\tan\beta = 6$. The study of the pseudoscalar A_0 at resonance is an excellent starting point for the search for new physics. Complementarily, we investigate the total production and potential discovery of the A_0 particle through the signal processes $gg \to A_0 \to WW \to X_W$ and $gg \to A_0 \to t\bar{t} \to WbW\bar{b} \to X_W b\bar{b}$. In Tables IX–X and XII–XIII, we provide the cross sections generated for the SM background processes and the corresponding signals at the different hadron colliders. Finally, in Tables XI and XIV, we present the number of expected events for the signals $gg \to A_0 \to W^+W^- \to X_W$ and $gg \to A_0 \to t\bar{t} \to WbW\bar{b} \to X_W b\bar{b}$, where we have considered the dominant SM backgrounds. According to the data obtained, the production of the pseudoscalar A_0 at the LHC and FCC-hh through the $gg \to A_0 \to t\bar{t} \to WbW\bar{b} \to X_W b\bar{b}$ signal provides a suitable mechanism to study this particle. Our study complements other studies in the context of present and future hadron-hadron, hadron-lepton, and lepton-lepton colliders on the production and decay of the pseudoscalar A_0.

ACKNOWLEDGMENTS

E. C.-A. appreciates the postdoctoral stay at the Universidad Autónoma de Zacatecas, México. A. G.-R. and M. A. H.-R. thank SNII and PROFEXCE (México).

DATA AVAILABILITY

The data supporting this study's findings are available within the article.

APPENDIX: EFFECTIVE COUPLINGS IN THE BLHM

In this appendix, Tables XV–XVII present the effective couplings involved in our calculation of the production of the pseudoscalar A_0.

TABLE XV. Effective couplings involved in our calculation of the decay of the pseudoscalar boson A_0.

	Effective couplings
$g_{A_0t\bar{t}}$	$\frac{3c_\beta y_1 y_2 y_3}{\sqrt{y_1^2+y_2^2}\sqrt{y_1^2+y_3^2}} - \frac{2c_\beta s_\beta v y_2 y_3 (y_3^2-2y_1^2)}{f\sqrt{y_1^2+y_2^2}(y_1^2+y_3^2)} - \frac{3c_\beta s_\beta^2 v^2 y_1 y_2 y_3^3}{2f^2(y_1^2+y_2^2)^{5/2}(y_1^2+y_3^2)^{5/2}}$
	$\times\left(4y_1^6+4(2y_2^2+y_3^2)y_1^4+y_1^2(4y_2^4+8y_3^2y_2^2-2\sqrt{y_1^2+y_3^2})+y_2^2(4y_2^2y_3^2+\sqrt{y_1^2+y_3^2})\right)$
$g_{A_0b\bar{b}}$	$-c_\beta y_b$
$g_{A_0T\bar{T}}$	$-\frac{c_\beta s_\beta v y_1^2}{f(y_1^2+y_2^2)^{3/2}(y_1^2+y_3^2)(y_2^2-y_3^2)}\left(y_1^4(y_2^2+2y_3^2)+y_1^2(8y_2^2y_3^2-2y_3^4)-y_2^2(y_2^4+3y_2^2y_3^2-7y_3^4)\right)$
$g_{A_0T_5\overline{T_5}}$	$-\frac{9c_\beta s_\beta v y_1^2 y_2^2 y_3^2}{f(y_1^2+y_3^2)^{\frac{3}{2}}(y_3^2-y_2^2)}$
$g_{A_0T_6\overline{T}_6}$	$\frac{c_\beta s_\beta v y_1}{f}$
$g_{A_0T^{23}\bar{T}^{23}}$	$\frac{c_\beta s_\beta v y_1(3y_1^2-5y_3^2)}{f(y_1^2+y_3^2)}$
$g_{A_0A_0h_0}$	$-\frac{1}{2}v\lambda_0\sin(\alpha-\beta)\sin(2\beta)$

TABLE XVI. Vector and axial-vector coupling constants of the interaction vertex involving a gauge boson with a pair of fermions.

Vertex	Vector couplings	Axial-vector couplings
$\gamma t\bar{t}$	$g^V_{\gamma t\bar{t}} = \frac{2gs_W}{3}$	$g^A_{\gamma t\bar{t}} = 0$
$\gamma b\bar{b}$	$g^V_{\gamma b\bar{b}} = -\frac{gs_W}{3}$	$g^A_{\gamma b\bar{b}} = 0$
$\gamma T\bar{T}$	$g^V_{\gamma T\bar{T}} = \frac{2gs_W}{3}$	$g^A_{\gamma T\bar{T}} = \frac{gs_W v^2}{3f^2}(c_\beta^2 - \frac{y_1^2(4c_\beta^2(y_2^2-y_3^2)^2+s_\beta^2(2y_2^2+y_3^2)^2)}{(y_1^2+y_2^2)(y_2^2-y_3^2)^2} + \frac{s_\beta^2 y_3^2(y_2^2-2y_1^2)^2}{(y_1^2+y_2^2)^2(y_1^2+y_3^2)})$
$\gamma T_5\overline{T_5}$	$g^V_{\gamma T_5\overline{T_5}} = \frac{2}{3}gs_W$	$g^A_{\gamma T_5\overline{T_5}} = \frac{3gs_\beta^2 s_W v^2 y_1^2 y_2^2 (y_3^2-y_1^2)}{2f^2(y_1^2+y_3^2)^2(y_2^2-y_3^2)}$
$\gamma T_6\overline{T_6}$	$g^V_{\gamma T_6\overline{T_6}} = \frac{2}{3}gs_W$	$g^A_{\gamma T_6\overline{T_6}} = -\frac{3c_\beta^2 gs_W v^2}{4f^2}$
$\gamma T^{2/3}\overline{T}^{2/3}$	$g^V_{\gamma T^{2/3}\bar{T}^{2/3}} = \frac{2}{3}gs_W$	$g^A_{\gamma T^{2/3}\bar{T}^{2/3}} = \frac{gs_\beta^2 s_W v^2}{f^2}$

TABLE XVII. Continuation of Table XVI.

Vertex	Vector couplings	Axial-vector couplings
$Zt\bar{t}$	$g^V_{Zt\bar{t}} = \frac{g}{c_W}(\frac{1}{4} - \frac{2s_W^2}{3})$	$g^A_{Zt\bar{t}} = \frac{g}{4c_W}$
$Zb\bar{b}$	$g^V_{Zb\bar{b}} = \frac{g}{c_W}(-\frac{1}{4} + \frac{s_W^2}{3})$	$g^A_{Zb\bar{b}} = -\frac{g}{4c_W}$
$ZT\bar{T}$	$g^V_{ZT\bar{T}} = \frac{g}{6c_W}((3c_W^2 - s_W^2) - \frac{4s_W^2 v^2 y_1^2(4c_\beta^2(y_2^2-y_3^2)^2+s_\beta^2(2y_2^2+y_2)^2)}{f^2(y_1^2+y_2^2)(y_2^2-y_3^2)^2})$	$g^A_{ZT\bar{T}} = 0$
$ZT_5\overline{T_5}$	$g^V_{ZT_5\overline{T_5}} = -\frac{2gs_W^2}{3c_W}$	$g^A_{ZT_5\overline{T_5}} = \frac{3gs_\beta^2 v^2 y_1^2 y_2^2}{4c_W f^2(y_1^2+y_3^2)^2(y_2^2-y_3^2)^2}$
		$\times\big((s_W^2 y_3^4 - c_W^2(y_1^2(y_2^2+2y_3^2) - 2y_2^2y_3^2 + 5y_3^4))$
		$-c_W^2(y_1^2+y_3^2)(y_2^2-4y_3^2)\big)$

(Table continued)

TABLE XVII. *(Continued)*

Vertex	Vector couplings	Axial-vector couplings
$ZT_6\overline{T_6}$	$g^V_{ZT_6\overline{T_6}} = -\frac{g(8f^2 s_W^2 - 15c_\beta^2 c_W^2 v^2)}{12 c_W f^2}$	$g^A_{ZT_6\overline{T_6}} = -\frac{3gc_W c_\beta^2 v^2}{4f^2}$
$ZT^{2/3}\overline{T}^{2/3}$	$g^V_{ZT_{2/3}\bar{T}_{2/3}} = -(\frac{5gs_\beta^2 s_W^2 v^2}{3c_W f^2} + \frac{c_W g}{2} + \frac{7gs_W^2}{6c_W})$	$g^A_{ZT_{2/3}\bar{T}_{2/3}} = -\frac{gs_\beta^2 s_W^2 v^2}{c_W f^2}$
$W^+\bar{t}b$	$g^V_{W\bar{t}b} = \frac{g}{2\sqrt{2}}$	$g^A_{W\bar{t}b} = -\frac{g}{2\sqrt{2}}$
$W^+\bar{T}_5 b$	$g^V_{W\bar{T}_5 b} = -\frac{gs_\beta v y_2 (2y_1^2 - y_3^2)}{2\sqrt{2} f \sqrt{y_1^2+y_2^2}(y_1^2+y_3^2)}$	$g^A_{W\bar{T}_5 b} = \frac{gs_\beta v y_2 (2y_1^2 - y_3^2)}{2\sqrt{2} f \sqrt{y_1^2+y_2^2}(y_1^2+y_3^2)}$
$W^+\bar{T}_6 b$	$g^V_{W\bar{T}_6 b} = -\frac{\sqrt{2}c_\beta v y_2}{2f\sqrt{y_1^2+y_2^2}}$	$g^A_{W\bar{T}_5 b} = \frac{\sqrt{2}c_\beta v y_2}{2f\sqrt{y_1^2+y_2^2}}$
$W^+\bar{T}B$	$g^V_{W\bar{T}B} = \frac{g}{2\sqrt{2}}$	$g^A_{W\bar{T}B} = -\frac{g}{2\sqrt{2}}$
$W^+\bar{T}_5 B$	$g^V_{W\bar{T}_5 B} = -\frac{gs_\beta v y_1 (2y_2^2 + y_3^2)}{2\sqrt{2} f \sqrt{y_1^2+y_2^2}(y_2^2 - y_3^2)}$	$g^A_{W\bar{T}_5 B} = \frac{gs_\beta v y_1 (2y_2^2 + y_3^2)}{2\sqrt{2} f \sqrt{y_1^2+y_2^2}(y_2^2 - y_3^2)}$
$W^+\bar{T}_6 B$	$g^V_{W\bar{T}_6 B} = -\frac{\sqrt{2}c_\beta v y_1}{2f\sqrt{y_1^2+y_2^2}}$	$g^A_{W\bar{T}_5 B} = \frac{\sqrt{2}c_\beta v y_1}{2f\sqrt{y_1^2+y_2^2}}$

[1] G. Aad *et al.* (ATLAS Collaboration), Phys. Lett. B **716**, 1 (2012).
[2] S. Chatrchyan *et al.* (CMS Collaboration), Phys. Lett. B **716**, 30 (2012).
[3] A. Hayrapetyan *et al.* (CMS Collaboration), Phys. Lett. B **847**, 138290 (2023).
[4] G. Aad *et al.* (ATLAS Collaboration), Eur. Phys. J. C **83**, 496 (2023); **84**, 156(E) (2024).
[5] C. Englert, A. Freitas, M. M. Mühlleitner, T. Plehn, M. Rauch, M. Spira, and K. Walz, J. Phys. G **41**, 113001 (2014).
[6] M. Schmaltz, Nucl. Phys. B, Proc. Suppl. **117**, 40 (2003).
[7] N. Arkani-Hamed, A. G. Cohen, E. Katz, and A. E. Nelson, J. High Energy Phys. 07 (2002) 034.
[8] S. Chang, J. High Energy Phys. 12 (2003) 057.
[9] T. Han, H. E. Logan, B. McElrath, and L. T. Wang, Phys. Rev. D **67**, 095004 (2003).
[10] S. Chang and J. G. Wacker, Phys. Rev. D **69**, 035002 (2004).
[11] M. Schmaltz, J. High Energy Phys. 08 (2004) 056.
[12] M. Schmaltz and J. Thaler, J. High Energy Phys. 03 (2009) 137.
[13] M. Schmaltz, D. Stolarski, and J. Thaler, J. High Energy Phys. 09 (2010) 018.
[14] S. Godfrey, T. Gregoire, P. Kalyniak, T. A. W. Martin, and K. Moats, J. High Energy Phys. 04 (2012) 032.
[15] P. Kalyniak, T. Martin, and K. Moats, Phys. Rev. D **91**, 013010 (2015).
[16] J. M. Martínez-Martínez, A. Gutiérrez-Rodríguez, E. Cruz-Albaro, and M. A. Hernández-Ruíz, Chin. Phys. C **49**, 073101 (2025).
[17] E. Cruz-Albaro, A. Gutiérrez-Rodríguez, D. Espinosa-Gómez, T. Cisneros-Pérez, and F. Ramírez-Zavaleta, Phys. Rev. D **110**, 015013 (2024).
[18] E. Cruz-Albaro, A. Gutiérrez-Rodríguez, J. I. Aranda, and F. Ramírez-Zavaleta, Eur. Phys. J. C **82**, 1095 (2022).
[19] G. Aad *et al.* (ATLAS Collaboration), J. High Energy Phys. 08 (2024) 013.
[20] A. M. Sirunyan *et al.* (CMS Collaboration), J. High Energy Phys. 04 (2020) 171; 03 (2022) 187(E).
[21] G. Aad *et al.* (ATLAS Collaboration), Eur. Phys. J. C **85**, 573 (2025).
[22] M. Aaboud *et al.* (ATLAS Collaboration), Phys. Rev. Lett. **119**, 191803 (2017).
[23] G. Aad *et al.* (ATLAS Collaboration), J. High Energy Phys. 07 (2023) 203.
[24] A. Arhrib, S. Moretti, S. Semlali, C. H. Shepherd-Themistocleous, Y. Wang, and Q. S. Yan, Phys. Rev. D **109**, 055020 (2024).
[25] V. Chekhovsky *et al.* (CMS Collaboration), J. High Energy Phys. 10 (2025) 074.
[26] A. M. Sirunyan *et al.* (CMS Collaboration), Eur. Phys. J. C **79**, 564 (2019).
[27] A. M. Sirunyan *et al.* (CMS Collaboration), J. High Energy Phys. 03 (2019) 082.

[28] S. Chatrchyan *et al.* (CMS Collaboration), Phys. Rev. Lett. **112**, 171801 (2014).
[29] R. Contino and G. Servant, J. High Energy Phys. 06 (2008) 026.
[30] A. M. Sirunyan *et al.* (CMS Collaboration), J. High Energy Phys. 08 (2018) 177.
[31] G. Aad *et al.* (ATLAS Collaboration), J. High Energy Phys. 08 (2023) 153 and references therein.
[32] G. Aad *et al.* (ATLAS Collaboration), Eur. Phys. J. C **83**, 719 (2023) and references therein.
[33] R. L. Workman *et al.* (Particle Data Group), Prog. Theor. Exp. Phys. **2022**, 083C01 (2022).
[34] M. Aaboud *et al.* (ATLAS Collaboration), Phys. Lett. B **761**, 372 (2016).
[35] A. Hayrapetyan *et al.* (CMS Collaboration), J. High Energy Phys. 02 (2025) 089; Phys. Rep. **1115**, 368 (2025).
[36] I. Zurbano Fernandez, M. Zobov, A. Zlobin, F. Zimmermann, M. Zerlauth, C. Zanoni, C. Zannini, O. Zagorodnova, I. Zacharov, M. Yu *et al.*, High-Luminosity Large Hadron Collider (HL-LHC): Technical Design Report (CERN, 2020), ISBN 978-92-9083-586-8, 978-92-9083-587-5, 10.23731/CYRM-2020-0010.
[37] P. Azzi, S. Farry, P. Nason, A. Tricoli, D. Zeppenfeld, R. Abdul Khalek, J. Alimena, N. Andari, L. Aperio Bella, A. J. Armbruster *et al.*, CERN Yellow Rep. Monogr. **7**, 1 (2019).
[38] M. Cepeda, S. Gori, P. Ilten, M. Kado, F. Riva, R. Abdul Khalek, A. Aboubrahim, J. Alimena, S. Alioli, A. Alves *et al.*, CERN Yellow Rep. Monogr. **7**, 221 (2019).
[39] A. Abada *et al.* (FCC Collaboration), Eur. Phys. J. Spec. Top. **228**, 1109 (2019).
[40] R. Mammen Abraham, J. Adhikary, J. L. Feng, M. Fieg, F. Kling, J. Li, J. Pei, T. R. Rabemananjara, J. Rojo, and S. Trojanowski, J. High Energy Phys. 01 (2025) 094.
[41] M. L. Mangano, W. Riegler, M. Aleksa, P. P. Allport, S. Asai, A. Ball, M. I. Besana, E. R. Bielert, S. Bologna, E. Boos *et al.*, Conceptual design of an experiment at the FCC-hh, a future 100 TeV hadron collider, 10.23731/CYRM-2022-002.
[42] A. Abada *et al.* (FCC Collaboration), Eur. Phys. J. C **79**, 474 (2019).
[43] A. Abada *et al.* (FCC Collaboration), Eur. Phys. J. Spec. Top. **228**, 755 (2019).
[44] G. Aad *et al.* (ATLAS Collaboration), Phys. Rev. Lett. **108**, 111803 (2012).
[45] G. Aad *et al.* (ATLAS and CMS Collaborations), Phys. Rev. Lett. **114**, 191803 (2015).
[46] A. Arhrib, R. Benbrik, J. El Falaki, M. Sampaio, and R. Santos, Phys. Rev. D **99**, 035043 (2019).
[47] F. Abu-Ajamieh, S. Modak, S. Mukherjee, and S. K. Vempati, arXiv:2505.02092.
[48] J. I. Aranda, E. Cruz-Albaro, D. Espinosa-Gómez, J. Montaño, F. Ramírez-Zavaleta, and E. S. Tututi, J. Phys. G **44**, 105002 (2017).
[49] C. Kao, G. Lovelace, and L. H. Orr, Phys. Lett. B **567**, 259 (2003).
[50] A. S. Cornell, A. Deandrea, B. Fuks, and L. Mason, Phys. Rev. D **102**, 035030 (2020).
[51] M. M. Almarashi, Universe **7**, 392 (2021).
[52] E. Cruz-Albaro, A. Gutierrez-Rodrıguez, M. A. Hernandez-Ruız, and T. Cisneros-Perez, Eur. Phys. J. Plus **138**, 506 (2023).
[53] E. Cruz-Albaro and A. Gutiérrez-Rodríguez, Eur. Phys. J. Plus **137**, 1295 (2022).
[54] A. Gutiérrez-Rodríguez, E. Cruz-Albaro, D. Espinosa-Gómez, T. Cisneros-Pérez, and D. A. Pérez-Carlos, Nucl. Phys. **B1020**, 117134 (2025).
[55] R. L. Workman *et al.* (Particle Data Group), Prog. Theor. Exp. Phys. **2022**, 083C01 (2022).
[56] V. D. Barger and R. J. N. Phillips, *Collider Physics* (Addison-Wesley, New York, 1996); (Addison-Wesley, New York, 1997).
[57] E. Barradas, J. L. Diaz-Cruz, A. Gutierrez, and A. Rosado, Phys. Rev. D **53**, 1678 (1996).
[58] A. Denner and S. Dittmaier, Nucl. Phys. **B734**, 62 (2006).
[59] H. H. Patel, Comput. Phys. Commun. **197**, 276 (2015).
[60] H. H. Patel, Comput. Phys. Commun. **218**, 66 (2017).
[61] G. Aad *et al.* (ATLAS Collaboration), Eur. Phys. J. C **81**, 396 (2021).
[62] A. M. Sirunyan *et al.* (CMS Collaboration), J. High Energy Phys. 03 (2020) 055.